Mon. Not. R. Astron. Soc. **285,** 657–672 (1997)

A new class of rapidly pulsating star – IV. Oscillations in EC 20117 – 4014 and atmospheric analyses

D. O'Donoghue,[1,2] A. E. Lynas-Gray,[2] D. Kilkenny,[3] R. S. Stobie[3] and C. Koen[3]

[1]*Department of Astronomy, University of Cape Town, Rondebosch 7700, South Africa*
[2]*Department of Physics, University of Oxford, Nuclear Physics Laboratory, Keble Road, Oxford OX1 3RH*
[3]*South African Astronomical Observatory, PO Box 9, Observatory 7935, Cape, South Africa*

Accepted 1996 October 15. Received 1996 October 8; in original form 1996 June 17

ABSTRACT

A new class of pulsating stars, the EC 14026 stars, has recently been announced. We report the discovery of rapid oscillations in EC 20117 – 4014. The oscillations are multiperiodic with three periods detected so far: 137.3, 142.1 and 158.7 s. The peak-to-peak amplitude of these oscillations is ~ 1 per cent. Along with the spectrum and *UBV* colours, this implies that EC 20117 – 4014 is another member of the new class. Interestingly, there is evidence for period/phase changes in the main 137.3-s period, as no linear ephemeris can be found that will fit the collection of light curves we have obtained. We interpret the oscillations as pulsations of an sdB star in a binary with an F/G companion, as indicated by the optical spectra.

In order to derive atmospheric parameters of the component stars, low- (~ 3.5 Å) and intermediate- (~ 1 Å) resolution optical spectroscopy is presented for the first four EC 14026 stars to be discovered: EC 14026 – 2647, EC 10228 – 0905, EC 20117 – 4014 and PB 8783. Their spectra are modelled as the combination of sdB and F/G stars using a grid of high-gravity model atmospheres to represent the former, and observed spectra to represent the latter. The spectral types of the late-type companions are estimated to be in the range early F to early G. Atmospheric parameters for the sdB components of the four stars are derived and found to be similar: $\log g \sim 6.0$ and $T_{\rm eff} \sim 35\,000$ K. If the late-type companions are on or near the main sequence, their distances agree with those estimated for the sdB components, assuming that the masses of the latter are $\sim 0.5\,M_{\odot}$.

The evolutionary status of the four stars strongly suggests that the sdB component has suffered substantial mass loss by Roche lobe overflow, along the lines originally proposed by Mengel et al. This hypothesis can be tested by using the orbital time delay in the pulsations to measure the binary period and separation. The discovery of pulsations in sdB stars is important: asteroseismological studies to probe their structure and evolutionary time-scale can now be contemplated.

Key words: binaries: general – stars: individual: EC 20117 – 4014 – stars: individual: EC 14026 – 2647 – stars: individual: EC 10228 – 0905 – stars: individual: PB 8783 – stars: oscillations.

1 INTRODUCTION

In a companion paper (Kilkenny et al. 1997a, hereafter Paper I), a new class of variable stars, the EC 14026 stars, has been announced. The prototype, EC 14026 – 2647, displays 144-s oscillations with an amplitude of ~ 1 per cent. Low-resolution spectra and *UBV* colours suggest that the star is a composite, comprising a hot sdB star and a late-F or early-G companion. Its discovery inspired a search for similar oscillations in other stars of this kind. This has yielded seven additional oscillators to date, two of which have been sufficiently well studied to warrant publication: PB 8783 (Koen et al. 1997, hereafter Paper II) and EC 10228 – 0905 (Stobie et al. 1997b, hereafter Paper III). These objects also

appear to be binaries consisting of an sdB star and an F or early-G companion. They also show low-amplitude oscillations with periods in the range 122–153 s. The sdB star in PB 8783 has been identified as the source of the oscillations (Paper II). In this paper, we present the third star to be discovered (although the fourth to be reported), EC 20117 – 4014, and show that it is very similar to the others just mentioned.

In order to extract the maximum astrophysical information from these stars, parameters of the individual components are required. Using optical spectroscopy and photometry, a systematic investigation of the properties of these first four EC 14026 stars is presented in the second part of the paper. We conclude by discussing the evolutionary status of these stars and what might be learnt from the study of their pulsations.

2 EC 20117 – 4014

2.1 Basic data

A bright ultraviolet-rich star, EC 20117 – 4014, from the Edinburgh–Cape (EC) Blue Object Survey (Stobie et al. 1992, 1997a; Kilkenny et al. 1997b) has been identified at position $\alpha(1950.0) = 20^{h}11^{m}43\overset{s}{.}8$ and $\delta(1950.0) = -40°14'55''$ accurate to ~ 1 arcsec. Its magnitude and colours are $V = 12.47$, $B - V = 0.13$, $U - B = -0.69$, with uncertainties of ~ 0.01 mag (Kilkenny et al. 1997b). The *UBV* colours are similar to those of EC 14026 – 2647, which has $V = 15.28$, $B - V = 0.15$, $U - B = -0.84$ (Paper I).

Spectra of both stars, obtained at ~ 3.5-Å resolution with the South African Astronomical Observatory (SAAO) 1.9-m telescope and intensified Reticon spectrograph, are shown in Fig. 1. The spectra are similar, showing broad Balmer lines on a blue continuum, suggestive of an sdB star (Moehler et al. 1990). The presence of weak He I $\lambda\lambda$4471- and 4026-Å lines supports this interpretation. However, both stars also have the Ca II K line, which is not expected in stars as hot as sdB stars. This, along with the even lower excitation temperature *G* band in the spectrum of EC 14026 – 2647, strongly suggests that these are composite stars comprising an sdB primary with an F or a G companion. The *UBV* colours are consistent with this interpretation: the $B - V$ colours of sdB stars are usually negative. However, the addition of light from an F or a G companion will make an increasing contribution with wavelength to the

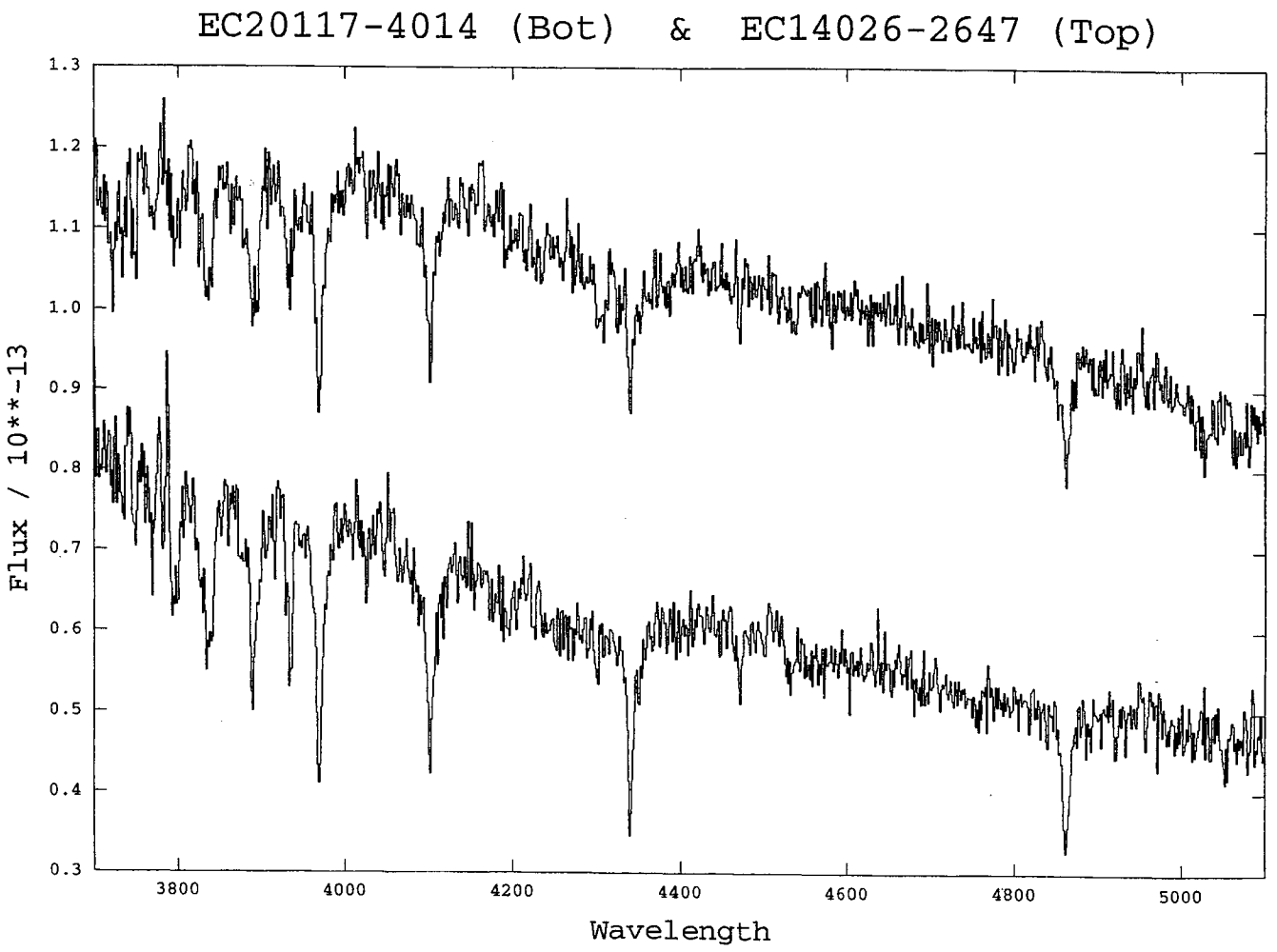

Figure 1. Spectra with ~ 3.5-Å resolution of EC 14026 – 2647 (top) and EC 20117 – 4014 (bottom). The ordinate scale, which is erg s^{-1} cm^{-2} $Å^{-1}$, is correct only for EC 20117 – 4014. The spectrum of EC 14026 – 2647 has been scaled to match that of EC 20117 – 4014 and then offset vertically by 5.0×10^{-14} erg s^{-1} cm^{-2} $Å^{-1}$.

Table 1. High-speed photometry and oscillation frequencies and amplitudes of EC 20117 – 4014.

Run Name	Date	Start of Run $JD_\odot$ (2440000.0+)	Length (hr)	f_1 (mHz)	a_1 (mmag)	f_2 (mHz)	a_2 (mmag)	f_3 (mHz)	a_3 (mmag)
S5860	29/05/95	9866.5563511	0.8						
S5861	30/05/95	9867.5391051	3.2	7.287(3)	3.4(2)	7.020(7)	1.4(2)	6.337(12)	0.9(2)[a]
ck121	31/05/95	9868.4910317	4.4	7.286(2)	3.4(2)	7.036(7)	1.2(2)	6.350(8)	1.0(2)
M9947a	17/08/95	9947.2347695	8.0	7.285(1)	3.6(2)	7.043(2)	1.4(2)	6.355(8)	0.7(2)
M9948a	18/08/95	9948.2328725	2.7	7.284(4)	3.2(2)	7.012(12)	1.0(2)	6.313(12)	1.0(2)
ck135	25/08/95	9955.3272932	4.2	7.286(2)	3.2(2)	7.030(6)	1.3(2)	-	-
ck137	27/08/95	9957.2514552	5.8	7.283(2)	3.8(3)	7.029(7)	0.8(2)	-	-
M9980a	19/09/95	9980.2648330	4.3	7.282(4)	3.4(4)	-	-	-	-
M0046a	24/11/95	10046.2646586	1.0						

[a]Errors are in brackets and are in units of the last significant figure of the corresponding tabulated value.

colours and explain the position of these stars in the *UBV* two-colour diagram (as clearly seen in Kilkenny et al. 1997b). Indeed, as discussed by Kilkenny et al. (1997b), these composite stars are commonly found in the EC survey.

2.2 Rapid variability

The similarity of the colours and spectrum of EC 20117 – 4014 to those of EC 14026 – 2647 prompted us to include it in our search for oscillations in other stars of this kind. High-speed photometry of EC 20117 – 4014 was obtained on a total of nine nights during the 1995 season. The observing log is listed in Table 1. The observations were obtained with the SAAO telescopes at Sutherland. The two systems used were the 0.75-m telescope with the University of Cape Town (UCT) High-Speed Photometer and the 1.0-m telescope with the St Andrews Photometer, in both cases with blue-sensitive S11 photomultiplier tubes. All observations were obtained in white light with a time resolution of 10 s. The response of the system thus has a similar effective wavelength to Johnson *B*, but with a much broader bandpass. Offset guiding enabled continuous monitoring of the programme star, except for occasional interruptions (about every 20–30 min) to obtain sky measurements. A cubic spline fitted to the sky values was interpolated to subtract the sky from the programme star readings. The data were then corrected for atmospheric extinction using a mean coefficient of 0.40 appropriate to stars of this colour observed at Sutherland. Finally, the data were normalized by the mean intensity during the run.

Periodic variability was suspected in EC 20117 – 4014 in a 45-min run of high-speed photometry on 1995 May 29 and confirmed on the following night. A portion of this latter light curve, S5861, is shown in Fig. 2. Oscillations with a period of 137 s and an amplitude of ~ 1 per cent are visible in the light curve. The oscillations are most obvious in the

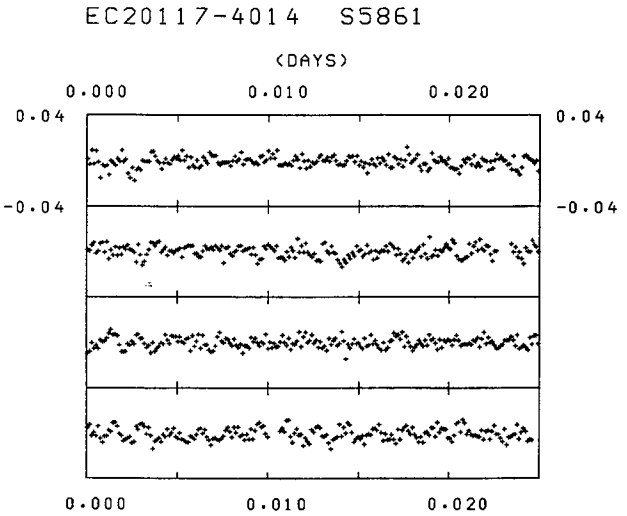

Figure 2. A portion of the light curve at 10-s time resolution in white light for EC 20117 – 4014 from run S5861 on JD 9867 (all four-digit Julian Dates should be understood to be offset from JD 244 0000). The ordinate scale is in intensity. 0.04 corresponds to a deviation of 4 per cent from the mean brightness during the run.

first and last panels of Fig. 2, and are lower in amplitude in the centre panels. This suggests that more than one frequency is present and that beating is taking place.

The spectral features and *UBV* colours, as well as rapid oscillations of similar period and amplitude, conclusively establish that EC 20117 – 4014 is an EC 14026 star.

Periodograms were calculated for all the runs in Table 1 using the techniques of Balona (1983) and of Deeming (1975) modified by Kurtz (1985). Both techniques gave the same results. The frequency range from 0 to the Nyquist frequency of 50 mHz was searched for periodic signals. No

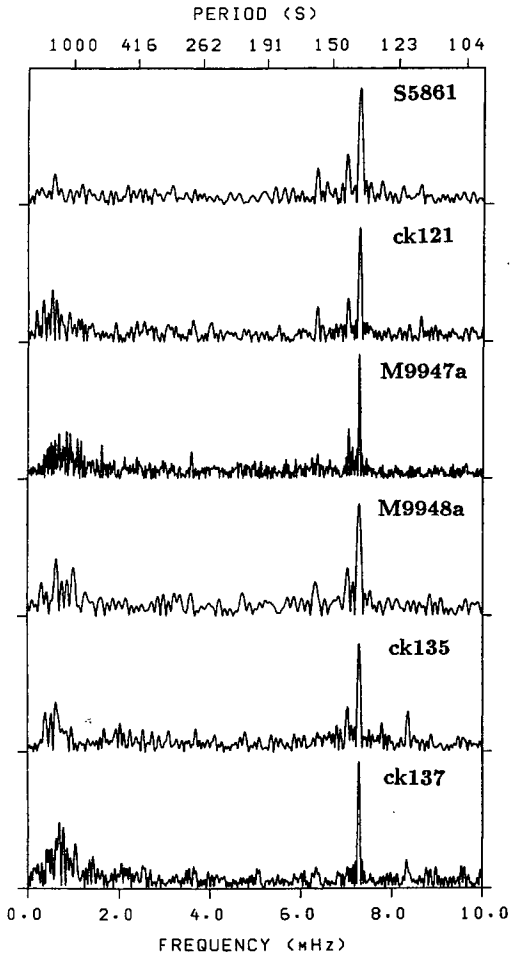

Figure 3. Periodograms of high-speed photometry of EC 20117 – 4014 in order from top to bottom JD 9867, 9868, 9947, 9948, 9955 and 9957. The corresponding runs (Table 1) are indicated. The ordinate scale is the same for each periodogram and ordinate carets are spaced at intervals of 0.4 per cent.

significant power in the range 10–50 mHz was found, with a limit on the semi-amplitude of 0.3 mmag. Consequently, we confined our attention to the range 0–10 mHz.

The periodograms of the six longest nights of data are shown in Fig. 3 and the frequencies identified listed in Table 1. The power at low frequencies (< 1 mHz) is caused by residual atmospheric transparency variations not accounted for by the standard extinction law. This frequency region should thus be disregarded. The main oscillation frequency at $f_1 = 7.285$ mHz is clearly identified on all nights with constant amplitude from night to night of 3.5 mmag. However, there are lower amplitude frequencies present ($f_2 = 7.043$ mHz and $f_3 = 6.350$ mHz) with amplitudes of ~ 1 mmag. These components are most clearly seen in the top two panels of Fig. 3, and there is strong evidence that their amplitude is not constant: the peak at 6.35 mHz is lower in M9947a and absent in ck135 and in ck137; the peak at 7.04 mHz is absent (or barely detected) in ck137. It should be noted that the apparent frequency at 8.333 mHz present in the bottom two panels of Fig. 3 is spurious, as it corresponds to the drive period ($P = 119.7$ s) of the 0.75-m telescope.

There is tentative evidence for a significant peak at 3.58 mHz ($P = 279$ s). It is most obvious in run M9947a but appears in ck121 and M9948a as well. Some of the longer runs were truncated to the same length, and periodograms calculated and combined to form an average periodogram (Fig. 4). The evidence for the 3.58-mHz peak is still present. Note that it is slightly but significantly different from half the frequency of the main peak. We regard the presence of this signal as unproven at the moment but suggest that it be searched for in future data sets. No peaks other than those already discussed were found down to a level of 0.4 mmag. We also searched for the harmonic ($2f_1$) of the main oscillation frequency and none was found above a level of 0.4 mmag.

In order to refine the frequency of the main oscillation we combined the data from different nights in groups. In com-

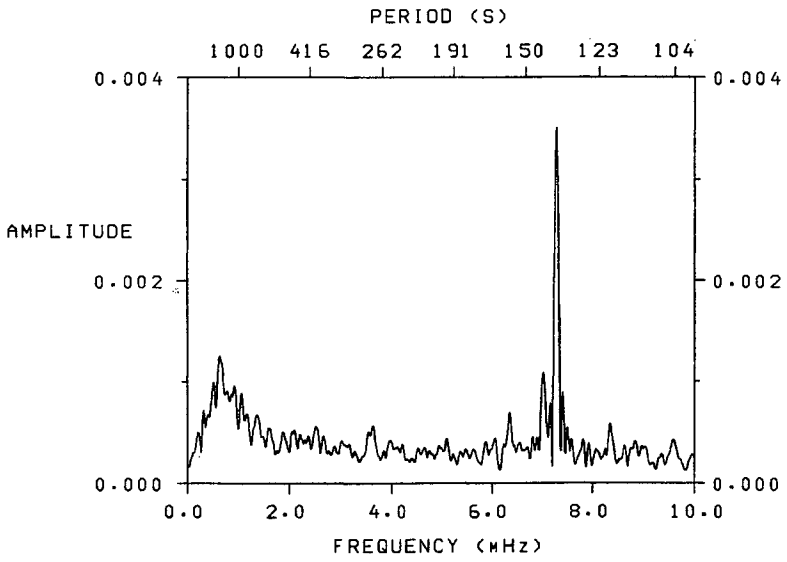

Figure 4. Average periodogram from a combination of runs S5861, ck121, M9947a, ck135 and ck137.

bining the four nights in 1995 August (JD 244 9947–9957) there was no cycle count ambiguity and the frequency derived was $f_1 = 7.284\,94 \pm 0.000\,02$ mHz with amplitude 3.54 ± 0.12 mmag. Combination of the three nights in 1995 May (JD 244 9866–9868) led to a frequency of $f_1 = 7.286\,68 \pm 0.000\,14$ mHz with amplitude 3.46 ± 0.15 mmag. The amplitudes are clearly the same within the errors, but the frequencies are not (the errors are non-linear least squares error estimates which, as is commonly known, underestimate the true errors). Nevertheless, this evidence for variable frequency, or equivalently variable phase, is unambiguous and is shown in Fig. 5 where pairs of nights have been combined. The multiple peaks in each of the four amplitude spectra in this plot arise from aliasing. If the same frequency could be fitted to each data subset, there would be at least one peak at the same frequency in each of the four spectra. It is clear that the aliases in the top two panels (derived from the 1995 May data), show a different frequency from the bottom two panels (derived from the 1995 August data). This conclusion was also supported by an (O – C) analysis. The times of maxima of the oscillation during the 1995 May data and the single night in November were compared with those expected from the best linear ephemeris derived from the August nights and large discrepancies were found. No single period was found that could fit the entire data set. Note that this conclusion is *not* due to the presence of the f_2 and f_3 components: these oscillations are of small amplitude, and in any case times of maximum for f_1 were derived from sections of data that were sufficiently long to resolve easily f_1 from f_2 and f_3.

3 SPECTROSCOPIC ANALYSES

In common with the other well-studied members of the EC 14026 class, EC 14026 – 2647 (Paper I), PB 8783 (Paper II) and EC 10228 – 0905 (Paper III), EC 20117 – 4014 exhibits short-period, low-amplitude oscillations. All four stars show evidence for a cooler companion (hereafter referred to as the 'late-type' star). Arguments are presented in Papers I and II, and discussed further below, that the oscillations arise in the sdB component and are due to stellar pulsation. It is clear that this emerging picture should be tested quantitatively for consistency. We shall thus embark on a spectroscopic analysis of all four stars to determine their fundamental parameters. It is especially important to determine effective temperatures and gravities of the sdB pulsators: these are key quantities in the pulsation analysis carried out in Paper III. The task is complicated by the fact that the observed spectra contain roughly comparable contributions from each of the components. The approach we adopted comprised the following.

(i) Computing a grid of high-gravity model atmospheres and Balmer line profiles to represent the spectrum of the sdB star. The grid spanned the range 20 000 to 40 000 K in $T_{\rm eff}$, 5.0 to 7.0 in $\log g$, and 0.0 to 0.3 in He abundance.

(ii) Using published 3.8-Å resolution spectra from the Jacoby, Hunter & Christian (1984) atlas to represent the late-type star. In addition, we also used our own higher resolution observations of a range of F and G stars.

(iii) Determining the spectral type of the late-type star and an estimate of the effective temperature and gravity of the sdB by fitting the sum of their spectra to the observations. The late-type star was then subtracted from the observed spectrum yielding that of the sdB star.

(iv) Fitting model Balmer line profiles to the sdB (residual) spectrum, thereby refining the estimate of $\log g$ and $T_{\rm eff}$ of the sdB star.

The procedure is illustrated in Fig. 6 which comprises four panels, one for each of the EC 14026 stars analysed. Each panel contains: (i) a spectrum from Jacoby et al. (1984) of the late-type star (bottom) determined in the analysis below to be the best match of the late-type star in the observed composite spectrum; (ii) the model for the sdB star (middle) with $T_{\rm eff} = 36\,000$ K and $\log g = 6.0$; and (iii) the top spectrum in each panel has two lines. The heavy line is the observed (lower resolution) spectrum of the EC 14026 star. The lighter line is the sum of the bottom and middle spectra. In spite of modest signal-to-noise ratio, a satisfactory fit to the observations of all four stars is apparent. In particular, note that the Ca II K line, which arises in the late-type star, is well reproduced by the model. The *G* band is prominent in the observed spectrum of EC 14026 – 2647, and also well reproduced by the model for this star. Fig. 7 shows similar modelling of the higher resolution observations (described in detail later). The signal-to-noise ratio and resolution in these plots are sufficient to reveal the weak metal lines of the late-type star, especially in the wavelength intervals between Hγ and Hδ, and Hδ and Hε. Comparison of the observations (heavy-line plots in Fig. 7) with the spectrum of the best-fitting late-type star (bottom) shows that virtually all of these weak features are seen in the EC 14026 stars. There can thus be no doubt that the interpretation of these stars as composite systems is correct.

We now consider the details of the individual steps. In Section 3.1, the observations are presented. In Section 3.2, the model atmosphere and line-profile computations are described. In Section 3.3, we discuss the technique we used for fitting the composite energy distribution and sdB Balmer line profiles.

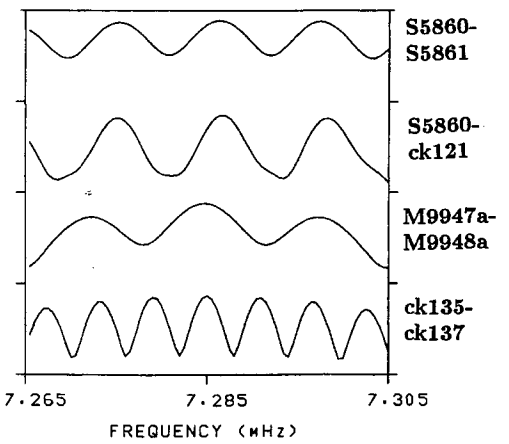

Figure 5. Periodogram detail for pairs of nights in the vicinity of the main peak at $f = 7.285$ mHz. The top spectrum is for JD 9866–9867 (S5860–S5861), the second from the top for JD 9866–9868 (S5860–ck121), the third for JD 9947–9948 (M9947a–M9948a) and the bottom for JD 9955–9957 (ck135–ck137).

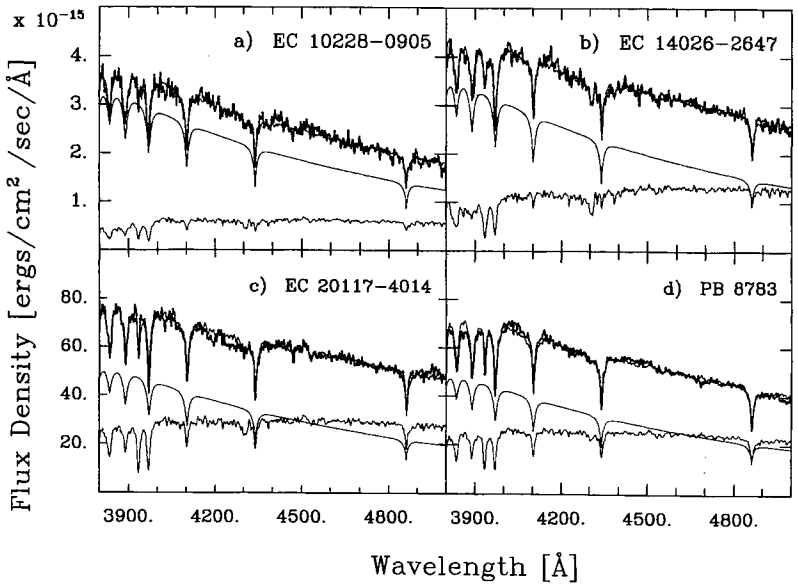

Figure 6. Grating 6 spectra for the first four EC 14026 stars. The best-fitting late-type star (from Jacoby et al. 1984) and a $\log g = 6$, $T_{\rm eff} = 35\,000$ K sdB model appear as the lower curves in each panel. The sums of these components are plotted as thin lines superimposed on the observations which are plotted as heavy lines. See text for more details.

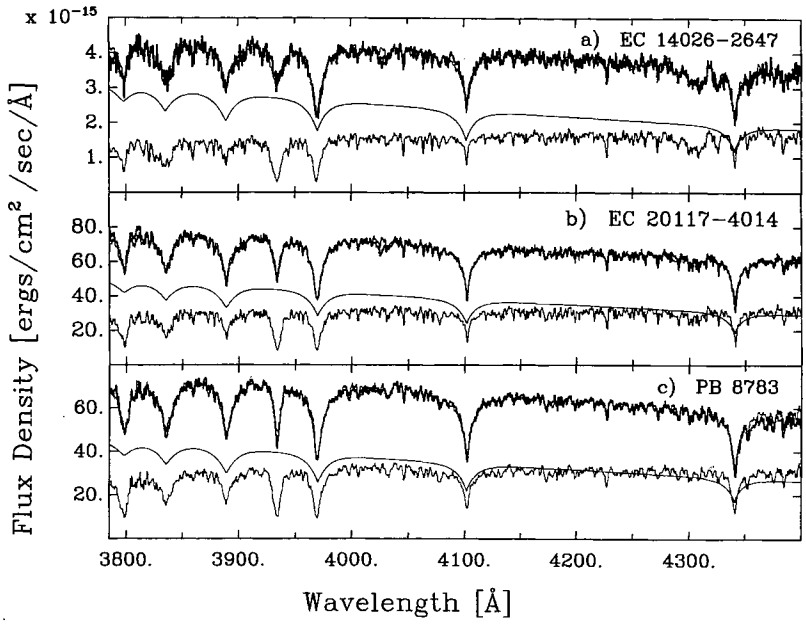

Figure 7. As for Fig. 6 except that the spectra were obtained with Grating 9 (resolution ~ 1.1 Å). The late-type stars are represented using the observations discussed in the text. Note the close correspondence between the metal lines in the observed composite spectrum and in the late-type star spectrum.

3.1 Spectroscopic observations

The observational material at our disposal consists of optical spectra obtained with the Image Intensified Reticon photon counting spectrograph (RPCS) attached to the SAAO 1.9-m telescope. In this system, the star is detected with one diode array while the sky is observed with the other. We began our analysis with the low-resolution (~ 3.5-Å) spectra acquired as part of the EC survey (Stobie et al. 1997a; Kilkenny et al. 1997b). These spectra were obtained with Grating 6, and covered the range 3400–5200 Å with exposure times of a few hundred seconds and a typical signal-to-noise ratio of 15–20. Subsequently, we realized that higher resolution was required and spectra were obtained with Grating 9, providing a resolution of 1.1 Å. For the Grating 9 data, it was necessary to use two grating angles to cover the wavelength range of the blue Balmer lines, so separate spectra were obtained for the 3800–4400 and 4600–5100 Å ranges. The signal-to-noise ratio obtained varied from 30 to over 100. A log of the

observations appears in Table 2. No higher resolution data are currently available for EC 10228 – 0905.

The spectra were reduced by standard techniques: pixel-to-pixel sensitivity variations were removed using flat-field spectra acquired at the beginning and end of each night; wavelength calibration was achieved using Cu–Ar arc spectra observed before and after each object spectrum. The dispersion relation was derived using a fifth-order polynomial yielding a wavelength scale accurate to 0.3 and 0.1 Å for Grating 6 and Grating 9 spectra, respectively.

As will be discussed below, the spectral fitting technique used the continuum slope of the observations. Thus flux calibration of the data is a significant issue. Relative calibration is all that is required and the standard technique is to derive the instrumental sensitivity from observations of spectrophotometric standard stars. This assumes that the light losses at the slit are wavelength independent while observing both the program star and the standard star. As it is impossible to rotate the slit of the RPCS to the parallactic angle, atmospheric dispersion along with variable guiding will ensure that slit losses are *not* wavelength independent at some level. We were able, however, to check the flux calibration using the *UBV* photometry of the program stars. We found that it was impossible to obtain a satisfactory flux calibraton for the Grating 9 spectra but that the Grating 6 spectra are accurate in this regard to better than several per cent. This was satisfactory for our purposes (at least in this first analysis). For the Grating 9 data, we achieved a flux calibration in the following manner: by using a cursor on a graphics display, we fitted a spline curve to the continuum of, on the one hand, the counts distribution for the Grating 9 spectra, and on the other, the flux distribution of the Grating 6 spectrum. The desired flux calibration was achieved by forcing these two continua to match.

It was found that the values of $\log g$ and $T_{\rm eff}$ derived for the sdB star depend very sensitively on the line profiles. The most reliable possible subtraction of the contribution of the companion from the observed Balmer lines is therefore required. For our Grating 9 spectra, the Jacoby et al. (1984) data could not be used in this regard as their resolution is lower by a factor of more than 3. Accordingly, during our 1995 November spectroscopic observing time we observed a range of bright stars of known spectral type with the same instrumental configuration with Grating 9 as used for the program stars in Table 2. The signal-to-noise ratio for these observations was $\sim$40–60 and the stars observed are listed

Table 2. Spectroscopic observations.

Object	Date	Grating	Wavelength Range (Å)	Resolution (Å)	Number Of Spectra	Exposure Time (s)
20117-4014	1991 Jul 14/15	6	3300–5200	3.5	2	200
	1995 Jul 26/27	9	3800–4400	1.1	2	1500
	1995 Jul 27/28	9	3800–4400	1.1	2	1500
		9	4600–5100	1.1	4	1500
		9	3800–4400	1.1	6	1200
	1995 Jul 28/29	9	4600–5100	1.1	4	1200
		9	3800–4400	1.1	7	1000-1200
	1995 Jul 30/31	9	3800–4400	1.1	10	1200
14026-2647	1989 Apr 26/27	6	3400–5200	3.5	2	500
	1992 Apr 4/5	6	3400–5200	3.5	2	500
	1995 Mar 3/4	6	3400–5200	3.5	2	1500
	1995 Jul 27/28	9	3800–4400	1.1	6	1500
	1995 Jul 28/29	9	3800–4400	1.1	6	1500
	1995 Jul 30/31	9	4600–5100	1.1	6	1200
		9	4600–5100	1.1	2	1250
10228-0905	1989 Apr 26/27	6	3400–5200	3.5	2	900
PB8783	1995 Jul 29/30	6	3400–5200	3.5	2	500
	1995 Nov 25/26	9	3800–4400	1.1	4	1500
	1995 Nov 27/28	9	3800–4400	1.1	4	1500

in Table 3. Again, these spectra could not be flux calibrated from the Grating 9 observations. The approach used with the program stars was also followed here where the counts distribution was forced to match a star of the corresponding spectral type from the Jacoby et al. (1984) atlas.

3.2 Modelling the sdB star

As mentioned above, the best possible modelling of the Balmer line profiles in theoretical energy distributions for sdB stars is needed. State-of-the-art models have been used by Saffer et al. (1994) to derive $\log g$ and $T_{\rm eff}$ from high-quality spectra of a large sample of sdB stars, but the emergent fluxes of these models have not been published. We were thus obliged to compute our own, the salient details of which will now be briefly described.

3.2.1 Balmer line broadening theory

Theoretical Balmer line profiles, used for comparison with absorption line profiles observed in stellar spectra, continue to be largely based on hydrogen Stark broadening tables by Vidal, Cooper & Smith (1973, hereafter VCS). Computer time considerations obliged VCS to restrict their tables (for Balmer lines) to Hα, Hβ, Hγ and Hδ. Furthermore, while Vidal et al. (1971, hereafter VCS1) found lower state interactions to be important in the cases of Hα and Hβ, VCS appear to imply that these could be neglected when calculating Stark broadening tables for Hγ and higher Balmer lines. Schöning & Butler (1989) extended VCS' tables to He II, but the present authors were unable to find published extensions of VCS tables (with or without lower state interactions) to the higher Balmer lines; Hε, H8, H9 and H10 were of particular interest, as they could be clearly seen in the EC 14026 star spectra.

In connection with Opacity Project work, Seaton (1990) gave further consideration to line profiles for transitions in hydrogenic ions; his requirements are that calculations should be fast and of sufficient accuracy for opacity work, for which line wings are of particular importance. Seaton calculated a basic matrix for electron perturbers using the Bethe–Born approximation, and showed this to be a good approximation (with some loss of accuracy in the far line wings) leading to normalized electron profiles having the correct form in both line cores and wings. For electrons, VCS used a unified classical path theory which reduces to the impact approximation in the line cores, and to the quasi-static approximation in the line wings. Seaton (1990) and VCS both adopted quasi-static theory for ion perturbers; this is known to give incorrect results in the line cores but should be satisfactory in the line wings. The essential difference between VCS' and Seaton's treatment of ion perturbers is that Seaton used equation-of-state considerations (Hummer & Mihalas 1988) to apply a cut-off in the far line wings, which takes some account of the eventual breakdown of quasi-static theory in this case.

Seaton's (1990) comparison between his theory and that of VCS (his fig. 5), as well as the comparison he makes with experiment, is extremely encouraging for both theories and suggests (for the purpose of the present study) that there is little to choose between them. VCS' theory was adopted for the present initial study of the EC 14026 star spectra because it is widely applied and associated computer programs are readily available.

In order to extend VCS' tables to higher Balmer lines (Hε, H8, H9 and H10), the VCS1 computer program was implemented in double precision on VAX/VMS computers. Hooper's (1966, 1968) low-frequency components of the electric microfield distribution were used, as tabulated by VCS1. VCS' modifications (their equations 9 and 10) were included in the VCS1 program implementation. Test calculations of Stark broadening (for Hα, Hβ, Hγ and Hδ) were compared with VCS' tables; some small differences were noted, although these never exceeded 0.1 per cent and had no effect on computed Balmer line profiles. The authors' VCS1 program implementation, as described above, was used by Dr M. Lemke for another project; the Stark broadening tables used here are his calculations, and include convolution with Doppler profiles that were made assuming all plasma constituents have the same temperature.

3.2.2 Theoretical Balmer line spectra for sdB stars

Model stellar atmospheres, in local thermodynamic equilibrium (LTE) and non-LTE, were computed and applied to the analysis of sdB star spectra by Heber et al. (1984) and Heber (1986); they resorted to non-LTE only for stars having $T_{\rm eff} \gtrsim 35\,000$ K. Kudritzki (1976) suggested (his fig. 3) that non-LTE is only essential at $T_{\rm eff} \approx 35\,000$ K if $\log g \lesssim 5.5$. More recent studies (Anderson 1985, 1989; Hubeny & Lanz 1995a, 1995b) introduced line-blanketing into non-LTE model stellar atmosphere calculations and illustrate its importance from the standpoint of theory. Cassinelli et al. (1995, 1996) failed to reproduce extreme ultraviolet ($500 \leq \lambda \leq 700$ Å) continua, observed in the early B-type giants ε CMa and β CMa with both LTE and non-LTE line-blanketed model atmospheres; in both cases, the LTE model gave the better (although still poor) fit.

The present authors were consequently persuaded to compute and use a grid of LTE line-blanketed model stellar atmospheres, ignoring possible non-LTE effects which would only be important at the highest $T_{\rm eff}$ and lowest $\log g$ values. Model stellar atmospheres were computed using ATLAS9 (Kurucz 1992) on a finely spaced grid $\{20\,000 \leq T_{\rm eff} \leq 40\,000$ K, $\Delta T_{\rm eff} = 2000$ K; $5.0 \leq \log g \leq 7.0$, $\Delta \log g = 0.5$; $0.0 \leq N({\rm He})/N({\rm H}) \leq 0.3$, $\Delta[N({\rm He})/N({\rm H})] = 0.1\}$ with metal abundances having solar values as proposed by Anders & Grevesse (1989); $N({\rm He})/N({\rm H})$ denotes the number density ratio of helium to hydrogen nuclei. As line-blanketing is dominated by metal lines, and metal abundances were held constant as $N({\rm He})/N({\rm H})$ was varied, the solar abundance $[N({\rm He})/N({\rm H}) = 0.1]$ opacity distribution function was used for all models.

Kurucz's (1992) program for calculating Balmer line profiles in LTE (BALMER9) is an adaptation of Peterson's (1969) code. For the present study, BALMER9 was modified so that Balmer line spectra (all Balmer lines between H10 and Hα being included, and all other lines excluded) could be computed for $3600 \leq \lambda \leq 6760$ Å; the new program was referred to as BALMERSP. No cut-offs were applied to the Balmer line wings in BALMERSP and the contribution of every line was included in the total line opacity (at each depth and wavelength point) before solving the radiative transfer equation;

in this solution, line scattering was included by adopting the Planck function (for every wavelength and temperature, appropriate to each depth point) as the line scattering source function.

The computed stellar atmospheres were used with BALMERSP to obtain corresponding theoretical sdB star spectra. Theoretical spectra computed with BALMERSP were in the form of monochromatic flux densities at the stellar photosphere. As the He I lines observed in the EC 14026 star spectra were extremely weak, and the adopted Balmer line broadening theory was among the best available, the theoretical energy distributions obtained with BALMERSP were expected to be good representations of the sdB star contributions to the observed flux-calibrated EC 14026 star spectra. Large-scale plots of the line profiles of Hγ to H8 were compared with those of Saffer et al. (1994: fig. 2); good overall agreement was found.

3.3 Fitting composite energy distributions

Fits to the observed EC 14026 energy distributions (i.e. the flux-calibrated spectra described above) were attempted with functions of the form

$$f(\lambda)=a_s f_s(\lambda)+a_l f_l(\lambda), \quad (1)$$

which gave monochromatic flux density predictions for wavelengths λ. Subscripts 's' and 'l' in equation (1) respectively correspond to contributions from the sdB and late-type components. If $f_s(\lambda)$ and $f_l(\lambda)$ are flux densities at the stellar photospheres, then the scaling factors a_s and a_l (assumed to be wavelength independent) are squared angular radii in radians; this is strictly true only if, as we assume, both stars are separated to the extent that neither affected the radiation field of the other, and no eclipse was underway at the epoch of observation.

An examination of the regression equation (1) showed there to be one dependent variable $[f(\lambda)]$, values for which were flux densities from observed spectra, and two independent variables $[f_s(\lambda)$ and $f_l(\lambda)]$; all three of these were subject to error. A standard least squares technique could not therefore be used to estimate a_s and a_l. Instead, the orthogonal distance regression package (ORDPACK) by Boggs et al. (1989) was used.

Table 3. Bright F/G stars observed with Grating 9.

Object name	Spectral Type
HR 692	F0V
HR 2677	F2V
HR 8646	F3V
HR 8859	F5V
HR 8843	F7V
HR 8635	G0V
HR 2493	G2V
HR 2882	G4V
HR 2261	G6V

The late-type companion contributions $[f_l(\lambda)]$ were obtained both from the flux-calibrated spectra of the stars listed in Table 3, and the flux densities of Jacoby et al. (1984) for solar metallicity main-sequence F and G stars. A radial velocity shift was applied to $f_l(\lambda)$ so that its Ca II K line was aligned in wavelength with the same line in the EC 14026 star spectra. It was also necessary to map the $f_l(\lambda)$ wavelength scale to be the same as that of the EC 14026 star spectrum being fitted.

The contributions from the sdB star $[f_s(\lambda)]$ were obtained from that theoretical spectrum in the grid which corresponded most closely to its current estimate of $T_{\rm eff}$ and $\log g$; while no radial velocity shift appeared to be necessary, the $f_s(\lambda)$ wavelength scale needed to be mapped to the wavelength scale of the EC 14026 star spectrum being analysed. Any metal lines contributed to the observed spectra by the sdB components could not be clearly distinguished from those of the late-type companions. As a consequence, convolving the broad Balmer lines in the theoretical sdB star spectra with either Grating 6 or Grating 9 instrumental profiles had no effect on comparisons with the observed spectra. Furthermore, convolution of the theoretical sdB star spectra with a rotation profile corresponding to $v \sin i = 50$ km s^{-1} had an effect that was just noticeable in the line cores; consideration of possible evolution scenarios made the choice of much larger $v \sin i$ values seem unreasonable. It was therefore decided that the theoretical sdB star spectra be used without instrumental or rotational broadening.

For each orthogonal distance regression, an initial value of $a_l = 0$ was chosen; this corresponded to a_s being set by normalization of $f_s(\lambda)$ to the observed flux as though the sdB star were the only significant contributor. Reasonable starting approximations to the sdB component $T_{\rm eff}$ and $\log g$ values were thus obtained because the sdB component makes the dominant contribution to the Balmer line wings owing to its higher gravity.

Depending on which EC 14026 star spectrum was being considered, three different types of orthogonal distance regressions were computed for each star.

(i) Grating 9 spectra were used for both $f(\lambda)$ and $f_l(\lambda)$; in this case the resolutions of both spectra were identical and no modification was required (note: because no Grating 9 spectra were available, this calculation was not performed for EC 10228 – 0905).

(ii) Grating 6 spectra were used for $f(\lambda)$ and Grating 9 spectra for $f_l(\lambda)$; in this case the Grating 9 spectra were convolved with a Gaussian ($\sigma = 1.4$ Å) to degrade their resolution to that of the Grating 6 spectra.

(iii) Grating 6 spectra were used for $f(\lambda)$ and Jacoby et al. (1984) spectra for $f_l(\lambda)$; in this case the Grating 6 spectra were convolved with a Gaussian ($\sigma = 1.8$ Å) to degrade their resolution to that achieved by Jacoby et al. (1984).

The observed flux densities in the Grating 6 and 9 spectra were weighted by the square root of the number of counts (attributable to the star) that were observed at the corresponding wavelength. The Jacoby et al. (1984) flux densities were assigned 10 000 counts at each wavelength point to correspond to the 1 per cent error that Jacoby et al. (1984) claim. The theoretical sdB star flux densities were assumed to be error free for the purpose of the orthogonal distance

regression calculations; as this was clearly not the case, the estimated errors in a_s and a_l were regarded as lower limits.

For each EC 14026 star, the three regression types were carried out with the chosen theoretical sdB star energy distribution and all available (between F0 V and G6 V) late-type star energy distributions; the adopted spectral type for the late-type companion was that resulting in the best agreement, in the sense of minimum χ^2, between the observed spectra and $f(\lambda)$ from equation (1). It was then possible to remove the late-type contribution from the observed EC 14026 star flux densities, leaving an estimate of the sdB star energy distribution.

The Balmer lines in this residual (sdB) spectrum were fitted with profiles from the grid of models to improve the estimates of $T_{\rm eff}$ and $\log g$ for the sdB star component. Within ranges defined by the grid of theoretical sdB star spectra, interpolation was used to obtain a theoretical sdB star spectrum for any $T_{\rm eff}$ and $\log g$ at a chosen N(He)/N(H); a non-linear least squares fit using the Levenberg–Marquardt algorithm (Marquardt 1963), as implemented in a program by Mr R. Ashley (UCT), then gave $T_{\rm eff}$ and $\log g$. The fitting procedure used a wavelength interval symmetrically disposed about each Balmer line rest wavelength, and extending sufficiently far to define adequately the continuum on either side of the line. Independent scaling factors for each Balmer line were used so that only the shape of the line profile (and not its normalization) determined the quality of the fit. The observed points were weighted using the square root of the number of counts attributable to the sdB component alone (i.e. with the contribution of the late-type star subtracted).

The improved estimates of $T_{\rm eff}$ and $\log g$ for the sdB star component then permitted a new iteration of orthogonal distance regression computations (as described above) to refine the estimates for $a_l f_l(\lambda)$. Three iterations were always sufficient to secure convergence i.e. no further changes in the parameters of equation (1).

Because of the exclusion of He I lines from the theoretical sdB star spectra, their weakness in the observed EC 14026 star spectra and the signal-to-noise ratio achieved, it was not possible to constrain the sdB component helium abundance; its influence on the theoretical energy distribution was largely compensated by a change in $\log g$. In view of the absence or weakness of He I lines in the observed spectra, the sdB component helium abundances were assumed to be zero for the purpose of the present study; this choice is quite consistent with earlier studies of field sdB stars (Heber et al. 1984). Saffer et al. (1994) find some sdB stars from their sample to be 'He-strong' (i.e. nearer to the solar value than is 'usual' for sdB stars) but the weakness of He I lines in the EC 14026 star spectra argue against their belonging to this group.

3.4 The nature of the EC 14026 binary systems

Derived $T_{\rm eff}$ and $\log g$ values for the sdB components, along with spectral types of their late-type companions, are listed in Table 4; these were derived from the minimum χ^2 orthogonal distance regression fits discussed above. The analyses of the Grating 6 spectra are distinguished in Table 4 by the inclusion of an '*' or 'J' in column 2; a 'J' indicates the use of the Jacoby et al. (1984) energy distributions to represent $f_l(\lambda)$ (hereafter referred to as the 'late-type companion template'). An '*' indicates the use of the observations of the stars listed in Table 3. Error limits entered in Table 4 are formal errors provided by the residual sdB spectra, and represent a lower limit on the true error.

Table 4. sdB star atmospheric parameters and spectral types for their late-type companions.

Star	Grating	$T_{\rm eff}$ (sdB)	$\log g$ (sdB)	Companion
	9			
EC 10228-0905	6*	33500 ± 900	6.00 ± 0.24	G2 V
	6J	35100 ± 900	5.70 ± 0.22	G0 V
	9	34700 ± 500	6.10 ± 0.13	G2 V
EC 14026-2647	6*	35900 ± 900	6.20 ± 0.20	G2 V
	6J	35200 ± 700	6.17 ± 0.16	G2 V
	9	34800 ± 300	5.87 ± 0.07	F5 V
EC 20117-4014	6*	34400 ± 700	5.82 ± 0.17	F5 V
	6J	36000 ± 800	6.19 ± 0.17	F6 V
	9	35700 ± 300	5.54 ± 0.07	F0 V
PB 8783	6*	38000 ± 800	5.80 ± 0.15	F0 V
	6J	36800 ± 540	5.75 ± 0.11	F3 V

The fits to the Grating 6 spectra of the four EC 14026 stars, obtained with the theoretical sdB energy distributions, and the Jacoby et al. (1984) energy distributions as late-type companion templates, are shown in Fig. 6. Fig. 7 shows the fits to the Grating 9 flux-calibrated spectra. The orthogonal distance regression scalefactors, when applied to the sdB star theoretical energy distributions and the late-type companion templates, clearly reproduce the observations.

A comparison between Figs 6 and 7 shows that unique fits were not obtained; in particular, the G2 V star contributions to the EC 14026 – 2647 flux near Hγ (Figs 6b and 7a) differ by roughly 60 per cent. Different contributions of the sdB and late-type companion star to the observed fluxes are largely (but not entirely) attributable to noise in the observations of the EC 14026 and late-type star template spectra, and additional noise introduced by flux calibration. The contributions of the late-type companion to the EC 20117 – 4014 flux near Hγ (Figs 6c and 7b) are in much better agreement, the signal-to-noise ratio being an order of magnitude higher in this case. While differences between the fits presented for the same star (in Figs 6 and 7) are clearly an indication of error inherent in the method, the general agreement between the results from the different fits (Table 4) is encouraging.

Several possible sources of systematic error were identified; these included the neglect of interstellar reddening, orbital motion in summing the spectra, and the presence of very weak He I (and other) lines contributed by the sdB components. Additional sources of error might have arisen through the assumption of solar metallicity in the sdB stars and their late-type companions. Furthermore, an inspection

of the observed spectra suggested the presence of higher Balmer lines (H11, H12,...) contributed by one or both components; these were not included in calculations of the theoretical sdB star energy distributions. We now consider these possible sources of error in more detail.

As discussed below, sdB stars with a main-sequence companion are believed to have evolved as a result of mass transfer; if this scenario is correct, the assumption of solar metallicity is unlikely to be correct and could have had unfortunate and unknown consequences for the analysis presented in this paper. The energy distributions used in the analysis were dependent, directly or indirectly, on the use of a solar abundance opacity distribution function in the sdB model atmosphere calculations; erroneous temperature structures could have resulted from incorrect line opacities based on a wrong metal abundance. There is therefore a need to improve the analysis techniques to the point where metal abundances of both components can be determined; these would provide important constraints on evolution scenarios. It must be stressed, however, that no evidence of an incorrect model atmosphere temperature structure was found from the fitting procedure described above.

Balmer lines higher than H10 were omitted from the calculation of the theoretical sdB star energy distributions; their wings may affect the other Balmer line profiles. The line most seriously affected was H10, and for this reason it was not used in $T_{\rm eff}$ and $\log g$ determinations. It was always possible to achieve a good fit with all other Balmer lines (H9, H8,..., Hβ), and so any distortion in H9 (and lower Balmer lines) due to the possible neglect of H11 and higher Balmer lines was regarded as unimportant in comparison with noise in the observed energy distributions. Seaton's (1990) treatment of hydrogen line broadening, when compared with experiment as shown in his figs 10–12, appears to give a proper description of level dissolution leading to a Balmer line confluence at the Balmer jump; his method might therefore be applied to constrain $T_{\rm eff}$ and $\log g$ for both components in the EC 14026 star binaries if high signal-to-noise ratio spectra could be obtained.

The neglect of very weak He I and other lines in the theoretical sdB star spectra was judged, from a close inspection of Fig. 7 (in particular), to have had a negligible effect on the fit achieved. No evidence of orbital motion was found during the addition of observed spectra taken several months apart (see Table 2) but only the lower resolution Grating 6 spectra were so widely spaced in time; the Grating 9 spectra for any given star were all obtained within 3 d. Thus, the Balmer lines shown in Figs 6 and 7 were not considered to have been significantly broadened as a result of possible orbital velocities of the two components. Orbital motions would be expected, however, and the inclusion of weak He I lines in the theoretical sdB star spectra would be crucial to their future measurement.

Interstellar extinction estimates for the four EC 14026 stars were obtained using maps made by Burstein & Heiles (1982); these are only strictly applicable to extragalactic objects and can provide only upper limits to $E(B-V)$ in the case of objects within the Galaxy. For high-latitude galactic objects, Burstein & Heiles maps give reasonable estimates of $E(B-V)$ if dust and gas are local and concentrated in the galactic plane. Estimates of $E(B-V)$ and $E(U-B)$ obtained from $E(B-V)$ following Hiltner & Johnson (1956), are presented in Table 5. From $E(U-B)$ values, it is clear that the energy distribution slopes in Figs 6 and 7 were in error by no more than 4 per cent as a result of the neglect of interstellar reddening; this was comparable with, or slightly less than, the flux-calibration errors discussed above. If significant, interstellar reddening would not have affected the $T_{\rm eff}$ and $\log g$ values derived for the sdB components as only line profiles were used; the spectral types assigned to the late-type companions, however, would have indicated an effective temperature that is too low.

Table 5. Interstellar reddening estimates.

Star	l	b	E(B – V)	E(U – B)
EC 10228-0905	253.87	39.17	0.03	0.02
EC 14026-2647	322.66	32.99	0.06	0.04
EC 20117-4014	0.81	−32.46	0.05	0.04
PB 8783	143.60	−66.66	0.00	0.00

Table 6. Comparison of estimated and observed V magnitudes.

Star	V Estimated	V Photoelectric	Source
EC 10228-0905	16.03	15.88	Paper III
EC 14026-2647	15.58	15.28	Paper I
EC 20117-4014	12.44	12.47	This paper
PB 8783	12.62	12.32	Paper II

As a consistency check, the fits to the observed energy distributions (Fig. 6) (which use Jacoby et al. spectra as templates for the late-type star energy distributions) were used to estimate V magnitudes, using the flux calibration of Cohen et al. (1992). The comparison with the observed photoelectric V magnitudes is presented in Table 6. In the case of PB 8783, the Grating 6 spectrum used in the flux calibration was obtained in conditions that were not perfectly photometric. Disagreement between the photoelectric and estimated V magnitudes for EC 14026 – 2647 arose through a probable underestimate of the G2 V star contribution, as discussed above. Otherwise, the estimated and photoelectric V magnitudes were consistent within the observational errors; the agreement was especially pleasing in the case of EC 20117 – 4014 for which high signal-to-noise ratio spectra were obtained.

A related consistency check involved distance determinations; estimates of the sdB and late-type companion distances, made independently, should agree. Angular radii of the sdB components were immediately obtained from normalization of the model fluxes represented by the $a_{\rm s}$ values; their distances then followed, calculated using radii from the derived surface gravities and an adopted mass of 0.5 $M_{\odot}$, as proposed by Saffer et al. (1994) and Saffer & Liebert (1995). Effective temperatures for the late-type companions were adopted from the spectral types (Table 4) deduced from the Fig. 6 fits. The transformation to effective temperature was made using the calibration proposed by

Habets & Heintze (1981: table 8); corresponding model atmosphere monochromatic flux densities, at the effective wavelength of the *V*-band filter (5450 Å), were obtained by interpolation in Kurucz's (1992) grid. The late-type companion angular radii then followed from their contributions to the observed *V*-band fluxes, estimated using the appropriate Jacoby et al. (1984) template star flux densities at 5450 Å after scaling by the corresponding a_1. The distances for the late-type companions were then obtained from the radii, using spectral types (Fig. 6 fits) and the Habets & Heintze (1981) calibration.

The derived angular radii and distances are listed in Table 7. Satisfactory agreement between the sdB and late-type companion star distances were achieved in all four cases. The distance to PB 8783 also agrees with the estimate in Paper II derived purely from photometry. If no eclipse was underway at the time of any observation, and both components are separated to the extent that neither significantly affects the radiation field of the other, one of two conclusions follows. The spectral decomposition analyses have either led to a consistent identification of the late-type companions as main-sequence stars (at least as far as their luminosity is concerned), or an incorrect sdB star mass was adopted. The position of the sdB components in the $\log g$–$T_{\rm eff}$ plane (discussed below) suggest that they are typical sdB stars. Saffer et al. (1994) and Saffer & Liebert (1995) find that the mean mass of a large sample of field sdB stars is 0.5 $M_\odot$ *with very little, if any, dispersion*. It was therefore concluded that the late-type companions, responsible for the observed Ca II K line and *G*-band features in the observed spectra, do indeed have main-sequence gravities and luminosities (but presumably different compositions).

Theissen et al. (1993) studied three binaries (PG 1718 + 519, 2110 + 127 and PHL 1079) each consisting of an sdB star with a late-type companion; the spectra shown in their fig. 4 show a remarkable resemblance to those in Fig. 6. EC 14026 – 2647 has *G*-band, Ca I λ4227-Å and Fe I λλ4325-, 4383-Å lines which appeared almost identical with those which Theissen et al. (1993) found in spectra of PG 1718 + 519 and 2110 + 127. Theissen et al. (1995) used colour excesses to assign spectral types of G6 and G7 to the late-type companions in PG 2110 + 127 and 1718 + 519 respectively; luminosity considerations led them to conclude that these late-type companions must be subgiants.

Because the spectrum of EC 14026 – 2647 appeared to be almost identical to those that Theissen et al. (1993) obtained for PG 1718 + 519 and 2110 + 127, the differences in the late-type companion spectral types derived from the three spectra were of some interest. As described above, an attempt was made to fit the observed EC 14026 – 2647 energy distribution using a G6 V template spectrum to represent the late-type companion; the result was not as satisfactory as the fits presented in Figs 6 and 7. The energy distribution analyses in the present paper were tightly constrained by the strength of the Ca II K line; unfortunately, this falls outside the wavelength range observed by Theissen et al.

Table 7. Angular radii and distances.

Star	Spectral Type	Angular Radius (radians)	Distance (pc)
EC 10228-0905	sdB	1.24×10^{-12}	2700
	G0 V	1.19×10^{-11}	2200
EC 14026-2647	sdB	1.28×10^{-12}	2600
	G2 V	1.34×10^{-11}	1900
EC 20117-4014	sdB	4.90×10^{-12}	680
	F6 V	4.15×10^{-11}	670
PB 8783	sdB	4.77×10^{-12}	700
	F3 V	3.43×10^{-11}	860

4 DISCUSSION

The atmospheric analysis of the four EC 14026 stars just described has shown them to be binaries, one component of which belongs to a fairly homogeneous set of sdB stars with $T_{\rm eff} \sim 35\,000$ K and $\log g \sim 6.0$, the other component of which is a main-sequence F or early-G star.

The oscillations seen in all four stars (Papers I–IV) have a narrow range of periods. General arguments are presented in Paper I that these oscillations are due to stellar pulsation in the sdB component. Paper II demonstrates that the oscillations arise in the sdB component of PB 8783. The values of $T_{\rm eff}$ and $\log g$ derived in this paper were used in Paper III to construct zero-age extreme horizontal branch (ZAEHB) models of the sdB components; the periods of low-order radial and low-degree non-radial pulsations of these models were found to be in good overall agreement with the observed periods (Paper III). We shall therefore adopt pulsations of the sdB star as the cause of the oscillations.

What is the evolutionary state of these stars? Before answering this question, a brief review of the status of sdB stars is needed. (More details can be found in Saffer & Liebert 1995.) There seems to be general consensus that, on the basis of their position in the $\log g$–$T_{\rm eff}$ plane (e.g. Greenstein & Sargent 1974, Saffer et al. 1994), the sdB stars are core He burning stars with hydrogen envelopes so thin ($q = M_{\rm core}/M_{\rm star} \gtrsim 0.98$) as to be incapable of sustaining hydrogen shell burning.

Exactly how the sdB stars evolved to this configuration is the subject of much debate. Stellar evolution teaches that red giant stars evolve, essentially 'instantaneously', into horizontal branch stars as soon as He burning is ignited in the core. This ignition takes place at roughly constant core mass $M_{\rm core} \sim 0.5\ M_\odot$. Although metallicity also plays a role, the distribution of stars on the horizontal branch is determined primarily by the mass of the overlying hydrogen envelope (Rood 1973; Iben & Rood 1970) that remains after He ignition: the thinner the hydrogen envelope, the bluer the horizontal branch star, and the closer is the value of q to 1.

The problem in explaining the sdB stars is how to reduce the mass of the hydrogen envelope in the red giant progenitor to such low levels ($q \gtrsim 0.98$) at exactly the time that core He burning is ignited. As the distribution of sdB stars in the

$\log g$–$T_{\rm eff}$ plane does not reach the He main sequence (which would imply the entire hydrogen envelope had been lost i.e. $q=1$), a finely-tuned mass-loss mechanism is needed.

The 'single-star' scenario (e.g. Heber et al. 1984) proposes that there is substantial mass loss at the top of the red giant branch caused by helium ignition. sdB stars would then be a continuation to $q\sim1$ of the classical horizontal branch stars. However, additional factors must also be considered: no gaps between the positions in the HR diagram of these two groups of stars would be expected. Yet Newell (1973) and (most recently) Saffer et al. (1994) have found a gap between the locus of field sdB stars and that of the field horizontal branch stars (seen also in Saffer & Liebert 1995). Moreover, gaps have also been seen in the distributions of the bluest horizontal branch stars, which are believed to be analogues of the field sdB stars, and the classical horizontal branch stars in old clusters such as NGC 6752 (Heber et al. 1986) and NGC 6791 (Liebert, Saffer & Green 1994).

Iben (1990) and Iben & Tutukov (1986, 1987), and references therein, have proposed an alternative view of the sdB stars as the result of mergers of low-mass He white dwarfs. The merged object will have sufficient mass to ignite He in the core and the evolutionary tracks place the objects in roughly the correct part of the HR diagram. However, a significant dispersion in the masses of the merged objects is expected which, as emphasized by Saffer et al. (1994), is not consistent with the very narrow distribution of sdB masses they find. Although the Iben & Tutukov scenario may explain the occasional sdB star (as well as the sdO stars which are much less homogeneous), it is difficult to see how the majority of sdB stars in the Saffer et al. and Saffer & Liebert (1995) samples can be explained in this way.

Mengel, Norris & Gross (1976) have also proposed a binary origin for the sdB stars as a means of explaining how most of the hydrogen envelope of the progenitor is removed. They suggest that sdB stars are the direct descendants of red giants which are transferring mass to a nearby companion. If He is ignited before the H envelope is lost, a classical horizontal branch star results. If the He envelope is lost before the core mass reaches that required for He ignition, a low-mass He white dwarf is formed. For binaries with initial separation $0.61<A<0.85$ au, mass transfer on to the secondary will remove almost the entire hydrogen envelope at the time that He ignites in the core, thereby producing an sdB star. A consequence recognized by Mengel et al. is that *all* sdB stars would have to be in binaries. In this scheme, 'fine tuning' is also required, as evidenced by the cited limits on the initial orbital separations; such separations have been criticized by Heber (1986) who argued that such wide binaries could not survive in globular clusters. Furthermore, the simulations of Liebert et al. (1994) led to the conclusion that the Mengel et al. mechanism produced far fewer sdB stars than seen in the old galactic cluster, NGC 6791. There is, however, increasing evidence (although contradicted by Saffer 1991) that a large number of sdB stars are in binaries (Ferguson, Green & Liebert 1984; Bixler, Bowyer & Laget 1991; Allard et al. 1994; Theissen et al. 1995; Ulla et al. 1995; Thejll, Ulla & MacDonald 1995; Kilkenny et al. 1997b). Indeed, Allard et al. (1994) and Ulla et al. (1995) argue that ~50 per cent of sdB stars may be in binaries. If this estimate is correct, the Iben & Tutukov explanation would be even harder to accept because of the large number of triple systems required to evolve to sdB binaries. All of these issues are thoroughly discussed in Bailyn et al. (1992), Liebert et al. (1994), Saffer et al. (1994) and Saffer & Liebert (1995).

4.1 The position of the sdB oscillators in the $\log g$–$T_{\rm eff}$ plane

In the $\log g$–$T_{\rm eff}$ plane (Fig. 8), the zero-age extended horizontal branch (ZAEHB) models of Caloi (1972) for $M_{\rm core}=0.5\,{\rm M}_{\odot}$ and He abundance 0.296 are shown labelled with the corresponding value of q. The He main sequence (He-MS) of Caloi (1972) is also shown, with numerical labels corresponding to the total stellar mass. The dotted line between the $q=0.999$ ZAEHB and 0.5-$M_{\odot}$ He-MS models is included to show the locus of models for $0.999<q<1$. Evolution of the ZAEHB is indicated by the solid line labelled 'Dorman' which is the track of a 'metal-poor' star with $q=0.994$, $M_{\rm core}=0.485\,{\rm M}_{\odot}$ from Dorman, Rood & O'Connell (1993: table 3). Two additional solid lines labelled 'Kawaler' are very recent unpublished post-ZAEHB evolutionary tracks kindly made available by Steve Kawaler; they have $M_{\rm core}=0.47\,{\rm M}_{\odot}$ and $q=0.999\,79$ and 0.999 89. The open symbols are the latest $\log g$ and $T_{\rm eff}$ (re)determinations for a large sample of sdB stars originally selected by Saffer et al. (1994) and recently refined and supplemented by Saffer & Liebert (1995) and Saffer (1996, private communication). As mentioned earlier, it is clear that the sdB stars have $M_{\rm core}\sim0.5\,{\rm M}_{\odot}$ and $q\gtrsim0.98$.

ZAEHB models (Sweigart 1987) and post-ZAEHB evolutionary tracks (Dorman et al. 1993; Caloi 1989) are also available. As illustrated in Saffer et al. (1994: fig. 5), the differences amongst these models are comparatively small. As the observational uncertainties in the determinations of $\log g$ and $T_{\rm eff}$ are currently larger, the models plotted in Fig. 8 should be regarded as 'representative', and were chosen for ease of plotting. In addition to the filled symbols, the models calculated by Steve Kawaler and used in Paper III are shown in Fig. 8 by the symbol 'X'.

The positions of the sdB components of the four EC 14026 stars discussed above are indicated by filled triangles in Fig. 8 (the Grating 9 results, which are expected to

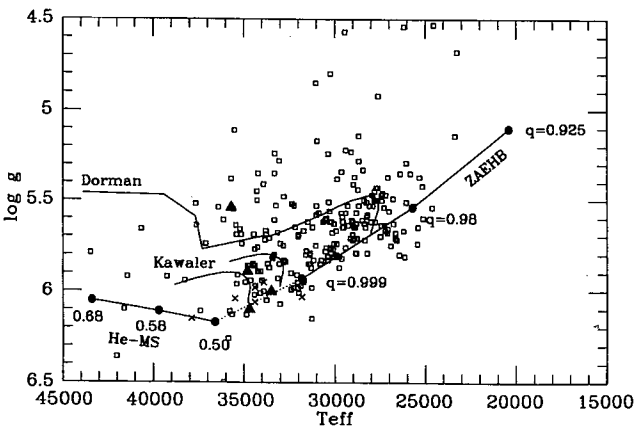

Figure 8. $\log g$–$T_{\rm eff}$ plane. The EC 14026 stars are represented by filled triangles. See text for other details.

be the most reliable, were used). With the exception of PB 8783, all stars lie near the ZAEHB with the thinnest of hydrogen envelopes ($q \gtrsim 0.999$). There is no evidence for differences between these sdB stars and the sample analysed by Saffer et al. (1994), Saffer & Liebert (1995) and Saffer (1996, private communication). In addition, it appears that the masses of the sdB components of the four EC 14026 stars are $\sim 0.5\,M_\odot$. Inspection of Table 4 shows that there is significant scatter in the results obtained with the different spectra of the program stars. We believe that this scatter is probably a realistic estimate of the true uncertainty in our determinations. As a result, the anomalous position of PB 8783 should not be regarded as significant, particularly in view of the fact that it has the hottest companion with the strongest Balmer lines. It is interesting that the temperature determinations of the four stars are consistent. It is obviously too early to say whether or not this is indicative of a 'pulsational instability strip', but this is an important question for the future.

4.2 The evolutionary status of the EC 14026 stars

Our analysis has shown that the late-type stars in the four systems under consideration are on the main sequence and have masses in the range 1.0–1.5 $M_\odot$. As just demonstrated, the sdB stars have $M \sim 0.5\,M_\odot$ and are more evolved. It is thus clear that the progenitor of the sdB star has lost a substantial amount of mass. A lower limit can be set by assuming that all the mass lost has been transferred on to the late-type star; the resulting limit is 0.25–0.5 $M_\odot$. In the calculation performed by Mengel et al., a binary with an orbital period of ~ 200 d and component masses 0.80 and 0.78 $M_\odot$, evolves via conservative Roche lobe overflow to being a binary with an orbital period of ~ 300 d, comprising a 0.5-$M_\odot$ sdB star and a 1.08-$M_\odot$ main-sequence star. The masses estimated for the components of the EC 14026 stars discussed above are in good agreement with this scheme.

If the binary separation is so wide that mass loss from the sdB progenitor by Roche lobe overflow has not taken place, the sdB progenitors would then have had to have lost between 0.5 and 1.0 $M_\odot$ by a 'single star' mass-loss mechanism. This is substantially larger mass loss than is believed to occur on the red giant branch of globular clusters (e.g. Jørgensen & Thejll 1993). The current evidence therefore favours mass loss by Roche lobe overflow. A definitive test can be made once the orbital periods are known and, as we will see in the next section, prospects for their determination are good.

The Mengel et al. hypothesis incorporates mass transfer at a rate sufficiently low to avoid common envelope evolution (e.g. Webbink 1979). Investigations of the importance of common envelope evolution in different kinds of binaries have been reported by Hjellming & Webbink (1987) and lucidly summarized in de Kool (1992) and de Kool & Ritter (1993). We believe (see next section) that the four systems discussed in this paper are not short-period binaries ($P_{\rm orb} \lesssim$ a few days) and therefore have *not* gone through common envelope evolution. Yet in order to accumulate an $\sim 0.5\,M_\odot$ He core, the sdB progenitor would have had to have ascended the giant branch and thereby developed a deep convective envelope. Roche lobe overflow in such a case is expected to be dynamically unstable (Mode III of Webbink 1979; de Kool 1992) and results in common envelope evolution. This apparent contradiction might be circumvented if the initial mass transfer were via Mode II and a transition to stable Mode III mass transfer took place (see de Kool & Ritter 1993 for further details). This issue requires further investigation.

We conclude this section by mentioning the problem of the 'coincidence' of He core ignition and the loss of almost all of the H envelope of the sdB progenitor. Unless this coincidence is removed, very few stars are expected to be produced by the Mengel et al. scheme (Iben & Tutukov 1987). If there were some (unspecified) mechanism by which He ignition in the form of a core flash could drive mass loss from the giant in a binary system, this would be a means of disposing of almost all the H-rich envelope of an sdB progenitor. Even though Jørgensen & Thejll (1993) advance convincing arguments against this notion on the basis of the morphology of (presumably mostly) single stars in globular cluster horizontal branches, the He flash may be far more effective as a means of mass loss if it occurs at the time that a star is almost overflowing its Roche lobe in a binary: the escape velocity at the surface of a Roche lobe filling star is, of course, zero. If so, the difficulties with the Mengel et al. hypothesis would then be removed as the remains of the H envelope would be lost as a direct result of He core ignition. If true, binaries with red giants which would otherwise have produced classical horizontal branch stars would now produce sdB/main-sequence systems.

Whether or not the above is the correct explanation, we feel that the extreme thinness of the H envelopes in the sdB stars is strongly suggestive of mass loss by Roche lobe overflow where the loss of the entire H envelope is a natural outcome of the process.

4.3 Binary sdB stars

The sdB pulsations in the four EC 14026 stars can be used as a probe of the binary: the variation in the light travel time as the sdB pulsator orbits the barycentre of the system will manifest itself as a variable phase of the oscillations. What can we expect to see? The semi-amplitude of the orbital time delay, a, for an sdB orbiting the barycentre of the binary is given by

$$a = 9.8 \frac{q'}{(1+q')} (P_{\rm orb})^{2/3} M^{1/3} \sin i \qquad \text{light-second},$$

where M is the total mass of the system in $M_\odot$, $P_{\rm orb}$ is the orbital period in days, q' is the mass ratio $M_{\rm l}/M_{\rm sdB}$ and i is the inclination of the system. (As before, the subscript 'l' refers to the late-type star.) Taking illustrative values of $M_{\rm sdB} = 0.5\,M_\odot$, $M_{\rm l} = 1.0\,M_\odot$ and $i = 30$, the value of a is listed in Table 8 for $P_{\rm orb} = 1$, 10, 100 and 1000 d. Measurement of the value of a for $P_{\rm orb} = 1$ d would be a challenging task, but not impossible for a star as bright as EC 20117 – 4014. Our O – C analysis shows that the typical 1σ error for measuring the time of maximum of the f_1 frequency from a 4000-s length of data is ~ 2 s. However, it is unlikely that the orbital period would be so short: theoretically, it is difficult to see how a binary such as EC 20117 – 4014 could emerge from the common envelope evolution implied by such a short orbital period; observationally, a 1-$M_\odot$ G star would

Table 8. Typical oscillation orbital time delay and radial velocity semi-amplitudes of EC 14026 stars (for $M_{sdB}=0.5\,M_\odot$, $M_1=1.0\,M_\odot$ and $i=30$).

P_{orb} (d)	a (s)	K_{sdB} (km s^{-1})	K_1 (km s^{-1})
1	3.7	82	41
10	17	38	19
100	80	18	9
1000	374	8	4

fill a substantial fraction of its Roche lobe and might show ellipsoidal variability or reflection effects from heating by its nearby hot companion. We have thus far found no sign of long-term variations in brightness of any EC 14026 star (but our constraints are weak). If the orbital period were 10 d or more, the orbital time delay would be easily measurable (unless the inclination were very small). The corresponding semi-amplitudes

$$K_{sdB}=210\,\frac{q'}{(1+q')}\left(\frac{M}{P_{orb}}\right)^{1/3}\sin i \quad \text{km s}^{-1}$$

$$K_1=210\,\frac{1}{(1+q')}\left(\frac{M}{P_{orb}}\right)^{1/3}\sin i \quad \text{km s}^{-1}$$

of their orbital radial velocity curves are also listed in Table 8, and show that if the orbital period is very short, it can be determined from a classical spectroscopic radial velocity study. Unless the system inclinations are uncooperative, prospects for determining P_{orb} for the EC 14026 stars are therefore good. With plausible estimates for the masses of the component stars, the binary separation, A, can then be derived and compared with the predictions of mass-transfer processes as described by Mengel et al. (1976), Webbink (1979), Hjellming & Webbink (1987) and de Kool & Ritter (1993).

Are the frequency/phase variations that have already been detected in the f_1 frequency of EC 20117 – 4014 due to orbital motion of the pulsator? Unfortunately the distribution of observations currently at hand is not sufficient to say whether or not orbital motion is responsible; a more comprehensive set of further observations will be required. None the less, an initial estimate is indicative. Suppose orbital motion is responsible. The frequency difference reported in Section 2.2 is 1.7 ± 0.5 μHz (we believe that this error estimate is realistic). Such a difference corresponds to a Doppler shift, $\Delta f/f$, of 2.4×10^{-4}, or a velocity difference of 70 ± 21 km s^{-1}. The mass of the late-type star in EC 20117 – 4014 is $\sim1.5\,M_\odot$. Assuming $P_{orb}\sim160$ d (twice the difference between the times of observation giving rise to the frequency difference), the resulting K_{sdB} is $36\sin i$ km s^{-1}, implying a peak-to-peak velocity difference (maximum blueshift to maximum redshift) of $72\sin i$ km s^{-1}. The observed frequency difference can thus be explained by orbital motion if $\sin i$ is ~1 and the observations took place half an orbital period apart at the times of maximum positive and negative radial velocity. Such special circumstances can be avoided if the orbital period were shorter or, in view of its substantial error of measurement, the true frequency difference were smaller than 1.7 μHz.

4.4 Asteroseismology of sdB stars

The pulsations in the EC 14026 stars can also be used as diagnostic probes of the pulsating star. First steps towards this are discussed in Paper II. Remarkable insight into the structure of white dwarfs has been gained from study of their pulsations by the Whole Earth Telescope (Winget et al. 1991, 1994). In particular, the compositional stratifications of the outer layers of the white dwarfs are being measured. A mature understanding of the pulsations in the EC 14026 stars may provide comparable insight into the structure of sdB stars: if it proves possible to measure the thickness of the surface hydrogen layer, it will significantly constrain the mass-loss mechanism in the progenitor.

The short periods seen in the EC 14026 stars offer the prospect of measuring, for the first time, the evolutionary time-scale of core He burning. Theoretical estimates suggest that this is $\sim10^8$ yr. Experience of trying to measure period changes in white dwarfs (Winget et al. 1991; Kepler et al. 1991) shows that if the periods of the EC 14026 stars are changing on this time-scale, a few years of observation will lead to a detectable period change and thus an observational check on this quantity. The evolution off the ZAEHB in Fig. 8 is initially at almost constant T_{eff} and decreasing $\log g$. This phase takes 100 Myr (Dorman et al. 1993). Subsequently, the star moves left in Fig. 8 but at a much more rapid rate: the time to increase T_{eff} to 37 500 K takes only 20 Myr. It is more likely, a priori, that sdB stars are in the first phase of evolution, during which an increase in the period might be expected. A rapid decrease in the periods of radial and non-radial p modes would be seen if the evolution was in the second of the phases just mentioned.

It is clearly important to check whether the pulsations in the sdB star are related to the binary nature of the EC 14026 stars so far studied. This can only be true if the structure of the sdB has been influenced by close binary evolution, especially mass exchange. We are thus searching a wide range of sdB stars, both binary and apparently single, for oscillations. The results of this survey will be presented in due course. Clearly, identification of the pulsation driving mechanism is an important goal. Although satisfactory overall agreement with the pulsation periods was attained, all the models constructed in Paper III were stable against pulsation driving. The answer to this question will provide additional insight into the structure and prior evolution of the sdB component.

ACKNOWLEDGMENTS

The authors are indebted to Dr M. Lemke for placing his extended hydrogen Stark broadening tables at our disposal; this saved considerable computer time. Mr R. Ashley (of the University of Cape Town) kindly placed his non-linear least squares Balmer line-profile-fitting program at our disposal. Rex Saffer kindly provided his latest determinations of $\log g$ and T_{eff} plotted in Fig. 8 in advance of publication and Seve Kawaler kindly made his unpublished post-ZAEHB evolu-

tionary models available to us. DOD acknowledges helpful conversations with Professors M. W. Feast and I. Iben, as well as the Oppenheimer Trust and the PPARC Astrophysics Visitors' Grant for financial support whilst visiting Oxford. He also thanks Dr John Menzies for timely access to the GODOT abacus.

REFERENCES

Allard F., Wesemael F., Fontaine G., Bergeron P., Lamontagne R., 1994, AJ, 107, 1565
Anders E., Grevesse N., 1989, Geochim. Cosmochim. Acta,, 53, 197
Anderson L. S., 1985, ApJ, 298, 848
Anderson L. S., 1989, ApJ, 339, 558
Bailyn C. D., Sarajedini A., Cohn H., Lugger P. M., Grindlay J. E., 1992, AJ, 103, 1564
Balona L. A., 1983, SAAO Circ., 7, 1
Bixler J. V., Bowyer S., Laget M., 1991, A&A, 250, 370
Boggs P. T., Donaldson J. R., Byrd R. H., Schnabel R. B., 1989, ACM Trans. Math. Softw., 5, 348
Burstein D., Heiles C., 1982, AJ, 87, 1165
Caloi V., 1972, A&A, 20, 357
Caloi V., 1989, A&A, 221, 27
Cassinelli J. P. et al., 1995, ApJ, 438, 932
Cassinelli J. P. et al., 1996, ApJ, 460, 949
Cohen M., Walker R. G., Barlow M. J., Deacon J. R., 1992, AJ, 104, 1650
Deeming T. J., 1975, Ap&SS, 36, 137
de Kool M., 1992, A&A, 261, 188
de Kool M., Ritter H., 1993, A&A, 267, 397
Dorman B., Rood R. T., O'Connell R. W., 1993, ApJ, 419, 596
Ferguson D. H., Green R. F., Liebert J., 1984, ApJ, 287, 320
Greenstein J. L., Sargent A., 1974, ApJS, 28, 157
Habets G. M. H. J., Heintze J. R. W., 1981, A&AS, 46, 193
Heber U., 1986, A&A, 155, 33
Heber U., Hunger K., Jonas G., Kudritzki R. P., 1984, A&A, 130, 119
Heber U., Kudritzki R. P., Caloi V., Castellani V., Danziger J., Gilmozzi R., 1986, A&A, 162, 171
Hiltner W. A., Johnson H. L., 1956, ApJ, 124, 367
Hjellming M. S., Webbink R. F., 1987, ApJ, 318, 794
Hooper C. F., 1966, Phys. Rev., 149, 77
Hooper C. F., 1968, Phys. Rev., 165, 215
Hubeny I., Lanz T., 1995a, ApJ, 439, 875
Hubeny I., Lanz T., 1995b, ApJ, 439, 905
Hummer D. G., Mihalas D., 1988, ApJ, 331, 794
Iben I., 1990, ApJ, 353, 215
Iben I., Rood R. T., 1970, ApJ, 161, 587
Iben I., Tutukov A. V., 1986, ApJ, 311, 753
Iben I., Tutukov A. V., 1987, ApJ, 313, 727
Jacoby G. H., Hunter D. A., Christian C. A., 1984, ApJS, 56, 257
Jørgensen U. G., Thejll P., 1993, A&A, 272, 255
Kepler S. O. et al., 1991, ApJ, 378, L45
Kilkenny D., Koen C., O'Donoghue D., Stobie R. S., 1997a, MNRAS, 285, 640 (Paper I, this issue)
Kilkenny D., O'Donoghue D., Koen C., Stobie R. S., Chen A., 1997b, MNRAS, in press
Koen C., Kilkenny D., O'Donoghue D., van Wyk F., Stobie R. S., 1997, MNRAS, 285, 645 (Paper II, this issue)
Kudritzki R. P., 1976, A&A, 52, 11
Kurtz D. W., 1985, MNRAS, 213, 773
Kurucz R. L., 1992, in Barbuy B., Renzini A., eds, IAU Symp. No. 149, The Stellar Populations of Galaxies. Kluwer, Dordrecht, p. 225
Liebert J., Saffer R. A., Green E. M., 1994, AJ, 107, 1408
Marquardt D. W., 1963, J. Soc. Industr. Appl. Math., 11, 431
Mengel J. G., Norris J., Gross P. G., 1976, ApJ, 204, 488
Moehler S., Richtler T., de Boer K. S., Dettmar R. J., Heber U., 1990, A&AS, 86, 53
Newell E. B., 1973, ApJS, 26, 37
Peterson D. M., 1969, Smithsonian Astrophys. Obs. Special Report No. 293
Rood R. T., 1973, ApJ, 184, 815
Saffer R. A., 1991, PhD thesis, Univ. of Arizona
Saffer R. A., Liebert J., 1995, in Koester D., Werner K., eds, Lect. Not. in Phys., White Dwarfs. Springer-Verlag, Berlin, p. 221
Saffer R. A., Bergeron J., Koester D., Liebert J., 1994, ApJ, 432, 351
Schöning T., Butler K., 1989, A&A, 219, 326
Seaton M. J., 1990, J. Phys. B, 23, 3255
Stobie R. S., Chen A., O'Donoghue D., Kilkenny D., 1992, in Warner B., ed., ASP Conf. Ser. 30, Variable Stars and Galaxies. Astron. Soc. Pac., San Francisco, p. 87
Stobie R. S. et al., 1997a, MNRAS, in press
Stobie R. S., Kawaler S. D., Kilkenny D., O'Donoghue D., Koen C., 1997b, MNRAS, 285, 651 (Paper III, this issue)
Sweigart A. V., 1987, ApJS, 65, 95
Theissen A., Moehler S., Heber U., de Boer K. S., 1993, A&A, 273, 524
Theissen A., Moehler S., Heber U., Schmidt J. H. K., de Boer K. S., 1995, A&A, 298, 577
Thejll P., Ulla A., MacDonald J., 1995, A&A, 303, 773
Ulla A., Thejll P., Hansen-Ruiz C. S., Rasilla J. L., Theissen A., MacDonald J., 1995, in Koester D., Werner K., eds, Lect. Not. in Phys., White Dwarfs. Springer-Verlag, Berlin, p. 272
Vidal C. R., Cooper J., Smith E. W., 1971, National Bureau of Standards Monograph 120 (VCS1)
Vidal C. R., Cooper J., Smith E. W., 1973, ApJS, 25, 37 (VCS)
Webbink R. F., 1979, in van Horn H. M., Weidemann V., eds, White Dwarfs and Variable Degenerate Stars. Univ. Rochester Press, Rochester, p. 426
Winget D. E. et al., 1991, ApJ, 378, 326
Winget D. E. et al., 1994, ApJ, 430, 839